31st Annual International Conference of the IEEE EMBS
Minneapolis, Minnesota, USA, September 2-6, 2009

3-D Microfabricated Electrodes for Targeted Deep Brain Stimulation

Noppasit Laotaveerungrueng, Chia-Hua Lin, Grant McCallum, Srihari Rajgopal, Charles P. Steiner, Ali R. Rezai, M.D., and Mehran Mehregany, Ph.D.

***Abstract*—This work presents a novel 4-sided, 16-channel deep brain stimulation electrode with a custom flexible high-density lead for connectivity with pulse generation electronics. The 3-dimensional electrode enables steering the current field circumferentially. The electrode is fabricated in pieces by micromachining and microfabrication techniques; the pieces are then assembled mechanically to form the electrode, after which the lead is connected. The electrode is modeled by finite element analysis and tested *in vitro* to validate the design concept, i.e., targeted stimulation. Simulation and experimental results for a targeted stimulation show close agreement. With a symmetric bipolar stimulation configuration, within a 3 mm radius, the electric potential in front of the activated side is at least 3.6 times larger than that on the corresponding two adjacent, not-activated sides, and 9 times larger than the corresponding opposite, not-activated side.**

I. Introduction

Deep brain stimulation (DBS) is a neurostimulation therapy treating symptoms of neurological disorders such as Parkinson's disease, essential tremor, major depressive disorder, and Tourette's syndrome [1]–[3]. DBS employs implanted electrodes within the brain that are connected to an implanted pulse generator which provides the stimulus to the desired neural structure. For Parkinson's disease therapy, the subthalamic nucleus (STN) is a highly effective area to place the DBS electrode [4]. However, since the brain anatomy varies from patient to patient, difficulties occur in positioning the electrodes using standard brain atlases and pre-implant neural recording sessions. Incorrect electrode placement limits treatment efficacy. The standard clinical DBS system utilizes cylindrical leads connecting to four circumferential electrodes. The uniform current distribution from these electrodes may result in undesirable side effects such as reduction of verbal fluency and executive functioning [5]–[7]. This paper presents a novel three-dimensional (3-D) electrode design containing sixteen distinct electrodes distributed equally on four sides of the lead assembly. The detailed structure is shown in Fig. 1. The distribution of electrodes on each side provides the ability to direct or steer the current field circumferentially. This paper is organized as follows: Section II describes the electrode and custom interconnect fabrication and assembly; Section III discusses simulation and test results; and the conclusion is presented in Section IV.

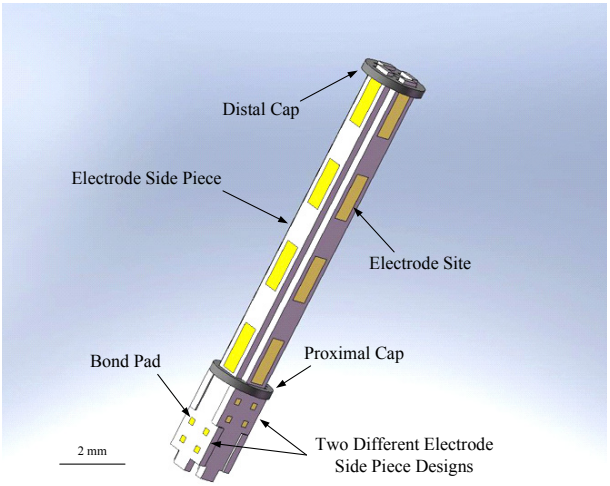

Fig. 1. Scaled rendition of the microfabricated DBS electrode. Metal traces from the bond pads to the electrode sites are not shown.

Manuscript received June 20, 2009.

N. Laotaveerungrueng, C.-H. Lin, G. McCallum, S. Rajgopal, and M. Mehregany are with the Department of Electrical Engineering and Computer Science, Case Western Reserve University, Cleveland, OH 44106 USA (e-mail: nxl30@case.edu).

C. Steiner and A. R. Rezai are with the Cleveland Clinic, Cleveland, OH 44195 USA.

II. Electrode And Lead Fabrication and Assembly

The 3-D electrode consists of four 824 µm x 11,500 µm side pieces, a distal cap, and a proximal cap. At the proximal end, the side pieces incorporate two complementary designs to accommodate bond pad size and spacing. Each side piece has four electrode sites, each 1500 µm x 500 µm in area, separated by 1300 µm gaps along the length. The electrode sites and metal traces are made of sputtered platinum. Each electrode site is connected to a bond pad by a 10 µm-wide metal trace; the lead is connected to the bond pads, which are 200 µm x 200 µm in area, separated by 400 µm gaps.

For the side pieces, fabrication began with a 250 µm-thick, double-side polished, p-type, (100) silicon wafer. A tri-layer insulator sandwich was deposited on the front side for substrate isolation using low pressure chemical vapor deposition (LPCVD): 300 nm-thick low-temperature silicon dioxide (LTO), followed by 150 nm-thick low-stress silicon nitride, followed by another 300 nm-thick LTO (Fig. 2(a)) [8], [9]. Such a dielectric stack structure has two advantages: (i) improved electrical insulation; and (ii) compensation of the competing stresses from the nitride and oxide layers.

The metal features were then realized using the lift-off process. A 5 µm-thick AZ9245 photoresist (PR) was spun on and patterned (MASK 1). A 10 nm-thick titanium adhesion layer and a 300 nm-thick platinum layer, were then sequentially sputtered. The lift-off process was accomplished by dissolving the PR in acetone overnight (Fig. 2(a)).

After patterning the metal, a 300 nm-thick silicon dioxide (Tetraethyl Orthosilicate or TEOS) film was deposited by LPCVD to passivate the metal traces (Fig. 2(b)).

A 10 μm-thick AZ9260 PR (MASK 2) was patterned to serve as an etch mask for opening windows in the passivation oxide to expose the electrode sites and bond pads; the oxide was etched by reactive ion etching (RIE) (Fig. 2(c)).

Next, two RIE steps were used to realize the side pieces (MASK 3). For this etch step, a 10 μm-thick AZ9260 PR coats was applied twice to serve as the etch mask: The first time for the first RIE step to etch through the tri-layer isolation/passivation (Fig. 2(d)); and the second time for the deep RIE (DRIE) step to etch through the 250 μm-thick silicon wafer (Figs. 2(e) and 3(a)).

In order to assemble the four side pieces into a 3-D electrode, two microfabricated distal and proximal caps were used as shown in Fig. 3(a) to the right of the two electrode side pieces (top and bottom, respectively). The jig to assemble the electrode was also microfabricated. The caps and jig were all fabricated on the same wafer in a one-mask DRIE step. The assembly jig consisted of two silicon pieces separated by four spacers. The top silicon jig piece had four rectangular through holes, for positioning the electrode side pieces. The assembly process to realize the 3-D electrode started with holding the four side pieces by four micromanipulators with vacuum tips. Next, the caps were

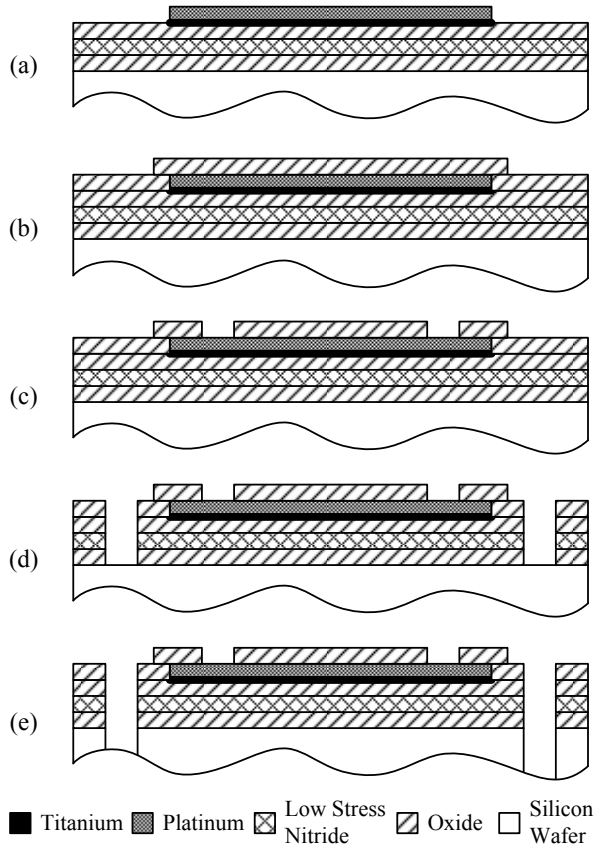

Fig. 2. Fabrication process flow for the 3-D electrode side pieces (not shown to scale): (a) Substrate isolation oxide/nitride/oxide layer with platinum on top (b) trace passivation oxide, (c) windows in the trace passivation layer to expose the electrode sites and bond pads; (d) isolation/passivation layers to expose the side piece outline; and (e) etching out the side piece from the wafer.

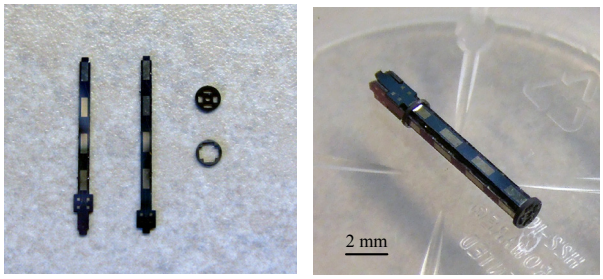

(a) (b)

Fig. 3. Optical photos of a microfabricated 3-D electrode: (a) Two electrode side pieces, a distal cap, and a proximal cap; and (b) an assembled electrode.

mounted from the top (distal end). Silastic (Dow Corning, Midland, MI) was used to glue the caps (Fig. 3(b)).

A custom flexible high-density lead was realized based on a modification of the MicroFlex Interconnect (MFI) technology [10]. The conventional MFI implementation consists of a flexible lead with gold ball bonds on vias for electromechanical contact between the microfabricated chip and the MFI substrate. Here, the ball bonds were replaced with epoxy beads. The flexible lead was fabricated by Microconnex, Inc. (Snoqualmie, WA). The base structure was a 50 μm-thick liquid crystal polymer (LCP). The metal traces and pads were realized in a dryfilm resist-based lift-off process from a 400 nm-thick gold layer on top of a 10 nm-thick TiW adhesion layer. A parylene overcoat was applied by chemical vapor deposition. Openings in the parylene on the bond pad area (for lead attachment to the electrode) were realized by patterning the dryfilm resist prior to parylene coating and ablating the parylene (by UV laser) that was deposited on the resist. As a final step, the resist was chemically removed. EPO -TECK H20E (Epoxy Technology, Billerica, MA) was used for the conductive epoxy beads. Figure 4 shows the DBS electrode connected to the lead.

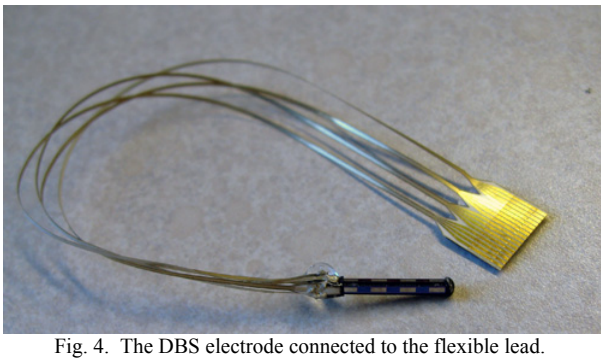

Fig. 4. The DBS electrode connected to the flexible lead.

III. Simulation and Experimental Results

Concept validation of the 16-site electrode was performed using COMSOL Multiphysics (v3.4) software to simulate the *in vitro* voltage field in a saline tank. The electrode was vertically placed in a saline tank modeled by a cylinder 7 cm in diameter and 7 cm in height. In the simulation, the conductivity of 0.9% sodium chloride solution was 1.5 S/m, representing the *in vivo* environment of the brain [11]. For bipolar stimulation, one of the electrode sites near the distal

end (Site #1) was excited with a 1-V DC signal, representing the pulse amplitude, and one site near the proximal end (Site #3) on the same flat piece was grounded (see Fig. 5).

For the *in vitro* experiment, the electrode was inserted from the bottom of a cylindrical glass container and placed vertically, approximately centered, as shown in Fig. 5. The container was 7 cm in diameter and 7 cm in height, and was filled with 0.9% sodium chloride. The recording electrode, a 170 mm-long Epoxylite-coated tungsten microelectrode (FHC, Bowdoin, ME), was placed from the top. Translation of the recording electrode was accomplished using a hydraulic oil micromanipulator (MO-95, Narishige International USA, East Meadow, NY). A stainless steel wire was wound around the beaker wall and served as a reference electrode for signal recording. A voltage-controlled symmetric bipolar stimulation configuration was implemented. A biphasic pulse generator (BPG-1, Bak Electronics, Mount Airy, MD) and a biphasic stimulus isolator (BSI-1, Bak Electronics) were used to generate stimulation pulses. The stimulation waveform was a 1 V, 500 µs cathodic pulse, followed by a 500 µs pulse-interval delay and a 500 µs anodic pulse. The period of the waveform was 7 ms. The stimulus was applied across the distal electrode Site #1 and #3 on one side shown in Fig. 5. Electrode Site #3 served as the return electrode. For recording, a differential amplifier with a headstage (Model 3000, A-M Systems, Carlsborg, WA) was used to amplify and filter the recorded signal with a 50x gain and 0.1 Hz to 20 kHz bandpass filter.

Figure 6(a) shows the measurement mapping plane across the electrode cross-section, cutting through the distal electrode site. Since the interface impedance is not purely resistive, the recorded signal would not be identical in pulse-shape to the stimulus. Indeed the recorded signal was parabolic and decayed toward 0 V. Thus, the peak of the cathodic phase was recorded and analyzed. Results are plotted in Figs. 6(b) to (e). These results show that, within a 3 mm radius, the electric potential in front of the activated side (Fig. 6(b)) was at least 3.6 times larger than the three other not-activated sides (Fig. 6(c)-(e)). However, the recorded voltage was much smaller than the applied stimulus due to the large frequency-dependent, electrode-electrolyte interface impedance between the platinum and saline [12]. In order to model the double-layer impedance at the interface

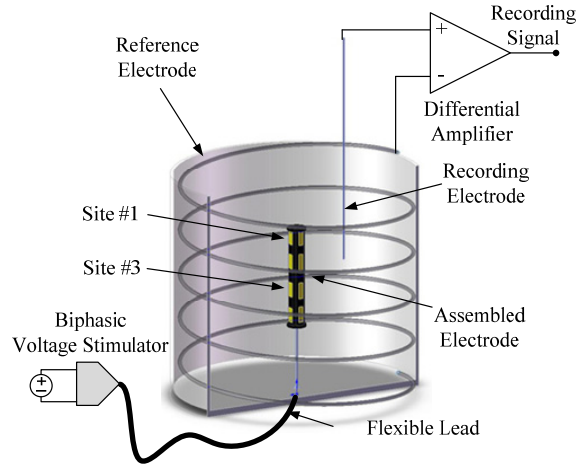

Fig. 5. The *in vitro* measurement setup (not to scale). The DBS electrode was inserted from the bottom, and the recording electrode was inserted from the top.

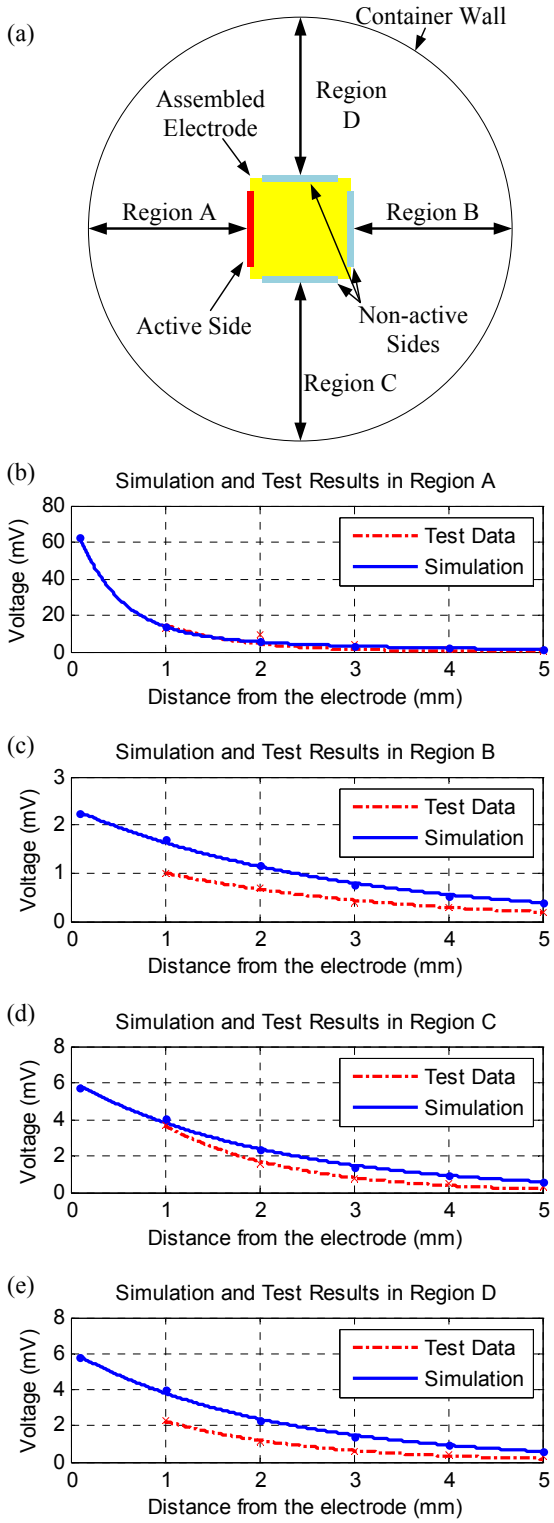

Fig. 6. Comparison of the simulation and test results: (a) Schematic of the mapping region in the measurement plane; (b) Region A; (c) Region B; (d) Region C; and (e) Region D.

between the electrode surface and the electrolyte in COMSOL, an additional 0.1 mm-thick film was placed on the surface of the electrode sites [11]. Since the model solution is only determined by the ratio of the conductivity and the thickness of this interface layer, the thickness was fixed and the conductivity was adjusted to fit the test data. The interface layer conductivity was adjusted to 0.05 S/m to fit the curve in Fig. 6(b), which is in close agreement to previous work [11]. The curve-fitting was achieved by MATLAB fitting-tool using an exponential function.

According to the simulation result, the applied voltage decreased from 1 V to 63 mV across the 0.1 mm (not the actual thickness) interface double-layer. Figure 7 shows the electric field contour from simulation. The electric potential range is from 563 mV to 500 mV, from electrode surface to the cylinder wall. However, in order to compare the *in vitro* testing and simulation results, the potential difference between the simulated result and the average potential near the cylinder wall, which was 500 mV, was used and plotted in Figs. 6(b) to (e). The simulation results indicated that within 1 mm of the electrode, the electric potential in front of the activated side is at least 8.2 times larger than the opposite (not activated) side and 3.4 times larger than the two adjacent (not activated) sides.

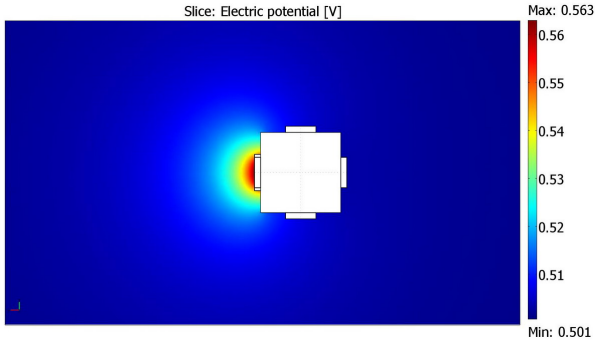

Fig. 7. The electric field contour from bipolar simulation on a cross-sectional plane of the electrode at the longitudinal center of the active site in Fig. 6(a).

The bipolar configuration was also used to estimate the electrode impedance by connecting a 1 kΩ resistor in series with the two electrodes placed in the saline tank. The current passing through the resistor was calculated and used to derive the total impedance, which includes two interface layer impedances, two metal trace interconnect impedances and the bulk saline [13]. The resulting total impedance, 2.3 kΩ, was larger than the impedance of the Medtronic DBS electrode which ranges from 0.5 to 1.5 kΩ [14]. This is due to the smaller electrode site and thinner metal interconnect used in this design.

IV. Conclusion

This paper presents preliminary results from a novel 3-D DBS electrode. Experiment and simulation results of the bipolar *in vitro* test show that the electric potential in front of the activated side is at least 3.6 times larger than the other three not-activated sides within a 3 mm radius. This electrode platform demonstrates the ability to concentrate the stimulation field in a targeted direction/region, while minimizing the stimulation of non-target areas. This platform also enables partial selective stimulation study of the STN, since once the 3-D electrode is positioned in the STN, current steering within 3 mm, comparable to the size of the STN, can be implemented. This would enable improved therapeutic benefit and reduced side effects, thereby greatly enhancing patient quality-of-life. In order to improve the performance of the electrode presented in this work, the current handling capability of the metal trace of each electrode site will be investigated in the future to deliver larger stimulation, while enhancing electrode life time. Additionally, redesigning the electrode dimensions will reduce the electrode-electrolyte interface impedance, thus decreasing the output impedance and increasing power efficiency. Other areas of investigation include long term reliability and *in vivo* experiment.

Acknowledgment

The authors would like to thank Prof. Dominique M. Durand of Case Western Reserve University for comments and suggestions on experimental setup, design and analysis.

References

[1] D. Chen, *et al.*, "Advances in neural interfaces: report from the 2006 NIH Neural Interfaces Workshop," *J. Neural Eng.*, vol. 4, pp. S137-S142, Sep. 2007.

[2] H. S. Mayberg, *et al.*, "Deep Brain Stimulation for Treatment-Resistant Depression," *J. Neuron.*, vol. 45, no. 5, pp. 651-660, 2005.

[3] J. S. Perlmutter and J. W. Mink, "Deep brain stimulation," *Annual Review of Neuroscience*, vol. 29, pp. 229-257, July 2006.

[4] A. L. Benabid, "Deep brain stimulation for Parkinson's disease," *J. Curr. Opin. Neurobiol.*, vol. 13, pp. 696–706, 2003.

[5] C. R. Butson and C. C. McIntyre, "Deep brain stimulation of the subthalamic nucleus: model-based analysis of the effects of electrode capacitance on the volume of activation," *Neural Engineering, 2005. Conference Proceedings. 2nd International IEEE EMBS Conference on*, pp.196-197, Mar. 2005.

[6] U. Schroeder, *et al.*, "Subthalamic nucleus stimulation affects a frontotemporal network: A PET study," *Annals of Neurology*, vol. 54, no. 4, pp. 445-450, Jul. 2003.

[7] K. Dujardin, *et al.*, "Influence of chronic bilateral stimulation of the subthalamic nucleus on cognitive function in Parkinson's disease," *J. Neurol.*, vol. 248, pp. 603–611, 2001.

[8] K. D. Wise, *et al.*, "Wireless implantable microsystems: High-density electronic interfaces to the nervous system," *Proc. IEEE*, vol. 92, no. 1, pp. 76–97, Jan. 2004.

[9] J. Wand, *et al.*, "A cochlear electrode array with built-in position sensing", in *Proc. 18th IEEE Int. Conf. Microelectromechanical Systems (MEMS 2005)*, pp. 786 – 789.

[10] J. U. Meyer, *et al.*, "High density interconnects and flexible hybrid assemblies for active biomedical implants," *IEEE Trans. Adv. Packag.*, vol. 24, pp. 366–374, 2001.

[11] S. Miocinovic, "Theoretical and experimental predictions of neural elements activated by deep brain stimulation", Ph.D. dissertation, Case Western Reserve University, Cleveland, 2007.

[12] R .W. de Boer and A. van Oosterom, "Electrical Properties of Platinum Electrodes: Impedance Measurements and Time-domain Analysis", *J. Medical & Biological Engineering & Computing*, vol. 16, no. 1, pp. 1-10, Jan. 1978.

[13] C. Lin, "A microfabricated deep brain stimulation electrode", MS thesis, Case Western Reserve University, Cleveland, 2009.

[14] C. R. Butson, C. B. Maks and C. C. McIntyre, "Sources and effects of electrode impedance during deep brain stimulation", *Clinical Neurophysiology*, vol. 117, no. 2, pp. 447-454, 2006.